5. R. Cauble *et al.*, *ibid.* **273**, 1093 (1996).
6. D. H. Kalantar *et al.*, *Phys. Rev. Lett.* **76**, 3574 (1996).
7. A. Carillon *et al.*, *ibid.* **68**, 2917 (1992).
8. J. A. Koch *et al.*, *ibid.*, p. 3291.
9. L. B. Da Silva *et al.*, *Opt. Lett.* **18**, 1174 (1993).
10. P. Jaegle *et al.*, in *X-ray Lasers 1994* (*AIP Conf. Proc. 332*, American Institute of Physics, New York, 1994), pp. 25–34.
11. J. Zhang *et al.*, *Phys. Rev. A* **54**, R4653 (1996).
12. B. J. MacGowan *et al.*, *Phys. Fluids B* **4**, 2326 (1992).
13. C. L. S. Lewis *et al.*, *X-Ray Lasers 1992*, E. E. Fill, Ed. (*Conf. Ser. 125*, Institute of Physics, 1992), pp. 23–30.
14. S. Basu *et al.*, *Appl. Phys. B* **57**, 303 (1993).
15. H. Daido *et al.*, *Phys. Rev. Lett.* **75**, 1074 (1995).
16. J. Nilsen and J. C. Moreno, *Opt. Lett.* **20**, 1387 (1995).
17. H. Daido *et al.*, *ibid.* **21**, 958 (1996).
18. Y. Li *et al.*, *Phys. Rev. A* **53**, R652 (1996).
19. C. H. Nam *et al.*, *Appl. Phys. B* **50**, 275 (1990).
20. J. Nilsen and J. C. Moreno, *Phys. Rev. Lett.* **74**, 337 (1995).
21. J. Zhang *et al.*, *Phys. Rev. A* **53**, 3640 (1996).
22. J. Zhang *et al.*, in preparation.
23. G. Cairns *et al.*, *Appl. Phys. B* **58**, 51 (1994).
24. J. Zhang *et al.*, *Phys. Rev. Lett.* **74**, 1335 (1995).
25. I. Weaver, thesis, Queen's University, Belfast (1996).
26. J. H. Scofield and B. J. MacGowan, *Phys. Scr.* **46**, 361 (1992).
27. J. Nilsen, in *Radiative-Hydro Modeling and Atomic Data Bases*, A. Hauer and A. L. Merts, Eds. (*AIP Conf. Proc. 168*, American Institute of Physics, New York, 1988), pp. 51–58.
28. This work is part of a program on x-ray laser research funded by the Engineering and Physical Science Research Council under grants GR/L 11540, 11946, 11779, and 11809. E.W. has been supported by the Austrian Fonds zur Förderung der Wissenschaftlichen Forschung under project number P10844 NAW. The work of the authors at Lawrence Livermore National Laboratory (LLNL) was performed under the auspices of the U.S. Department of Energy by LLNL under contract W-7405-Eng-48.

10 February 1997; accepted 25 March 1997

Local, Nonvolatile Electronic Writing of Epitaxial $Pb(Zr_{0.52}Ti_{0.48})O_3/SrRuO_3$ Heterostructures

C. H. Ahn, T. Tybell, L. Antognazza, K. Char, R. H. Hammond, M. R. Beasley, Ø. Fischer, J.-M. Triscone

A scanning probe microscope was used to induce local, nonvolatile field effects in epitaxial, ferroelectric $Pb(Zr_{0.52}Ti_{0.48})O_3/SrRuO_3$ heterostructures. Field-effected regions with linewidths as small as 3500 angstroms were written by locally switching the polarization field of the $Pb(Zr_{0.52}Ti_{0.48})O_3$ layer; the electronic density of the underlying metallic $SrRuO_3$ layer was modified and the sheet resistance was changed by up to 300 ohms per square. This procedure is completely reversible and allows submicrometer electronic features to be written directly in two dimensions, with no external electrical contacts or lithographic steps required.

Ferroelectric materials are characterized by a nonvolatile, reversible polarization field that has been successfully used in applications such as radiation hard memories (*1*). With advances in thin-film oxide growth, epitaxial conducting oxide–ferroelectric and high-temperature superconductor–ferroelectric heterostructures have recently been fabricated, and ferroelectric switching with improved fatigue properties has been observed, as have ferroelectric field effects in materials with relatively large carrier densities (*2–4*). Progress has also been made in the switching and imaging of the surface charge distribution and topographic deformations of small ferroelectric domains in bulk crystals and polycrystalline films using scanning force and optical probes (*5–8*).

Here, we investigated another opportunity afforded by the nonvolatile polarization of epitaxial ferroelectric oxides with high surface quality. We have devised a technique that produces a nonvolatile, local doping in a thin film using conducting oxide–ferroelectric heterostructures. This approach allows direct and reversible writing of submicrometer electronic structures by means of scanning probe microscopy; no permanent electrical contacts or lithographic processes are required, whereas existing electronic devices that use field effects require such contacts and lithography to achieve electronic doping. These local electronic nanofeatures also provide a detection mechanism to read out written ferroelectric domains that does not rely on the surface charge of the ferroelectric, which is susceptible to deterioration of contrast as a result of passivation.

A commercial atomic force microscope (AFM) with a metallized tip was scanned over the surface of an epitaxial ferroelectric $Pb(Zr_{0.52}Ti_{0.48})O_3$ (PZT)/$SrRuO_3$ heterostructure (Fig. 1) while a voltage was applied between the tip and the ultrathin metallic $SrRuO_3$ film. When the coercive field of the PZT layer was exceeded, the ferroelectric polarization switched directly underneath the tip and induced screening charges to flow in the $SrRuO_3$ layer, changing the total carrier concentration and hence the conductivity of the material.

We used epitaxial PZT/$SrRuO_3$ heterostructures that are well suited for application of a ferroelectric field effect and that can be grown with high quality and low roughness over large areas, which is important for these scanning experiments (*4*). For the growth of $SrRuO_3$, we carried out reactive molecular-beam epitaxy (MBE) in an ultrahigh-vacuum electron-beam evaporation system (*4*, *9*). X-ray diffraction patterns on thick (1000 to 5000 Å) samples revealed epitaxial growth of $SrRuO_3$(110) on $SrTiO_3$(001) substrates, with $SrRuO_3$ [001] parallel to $SrTiO_3$ [100]. The rocking curve taken around the 220 reflection has a full width at half maximum (FWHM) of 0.03°. Transport measurements taken on these films revealed large residual resistivity ratios (as high as 33). Ultrathin films were required for substantial field effects to be observed. Epitaxial metallic films (30 Å thick) were grown and characterized with in situ ultraviolet photoelectron spectroscopy (UPS), reflection high-energy electron diffraction (RHEED), and low-energy electron diffraction (LEED) measurements, followed by ex situ transport measurements. AFM images taken on these films revealed a root-mean-square surface roughness of 1.5 Å over a 6 μm by 6 μm area.

Afterward, tetragonal PZT was deposited onto the $SrRuO_3$ by means of off-axis radio frequency sputtering (*10*). X-ray diffraction revealed (001) growth on $SrRuO_3$, with PZT [100] parallel to $SrRuO_3$ [001]. The rocking curve of the PZT 001 reflection has a FWHM of 0.09°. For these films, the two ferroelectric polarization states lie perpen-

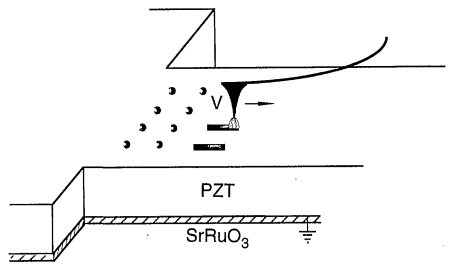

Fig. 1. Schematic of the PZT/$SrRuO_3$ heterostructure. With the use of an AFM with a metallized tip, ferroelectric domains can be polarized by applying a voltage between the tip and $SrRuO_3$ film that exceeds the coercive field of the PZT layer, resulting in a local, nonvolatile change in the electronic properties of the underlying film.

C. H. Ahn, T. Tybell, L. Antognazza, Ø. Fischer, J.-M. Triscone, Département de Physique de la Matière Condensée, University of Geneva, 24 Quai Ernest-Ansermet, 1211 Geneva 4, Switzerland.
K. Char, Conductus Inc., 969 West Maude Avenue, Sunnyvale, CA 94086, USA.
R. H. Hammond and M. R. Beasley, Department of Applied Physics, Stanford University, Stanford, CA 94305, USA.

dicular to the $SrRuO_3$ layer, with a remanent polarization of 10 to 15 $\mu C\ cm^{-2}$ and a coercive field of 70 to 100 $kV\ cm^{-1}$.

We first examined the writing and reading of ferroelectric domains in PZT by using the AFM as an electric field microscope. For these experiments, which were carried out in air and at room temperature, we used 1000 Å thick PZT [$Pb(Zr_{0.2}Ti_{0.8})O_3$ or $Pb(Zr_{0.52}Ti_{0.48})O_3$] films grown directly onto metallic Nb-doped $SrTiO_3$, with the substrate acting as a conducting ground plane. The measured roughness for these films is 2 Å over a 5 μm by 5 μm area, similar to that of the single-crystal substrate. Ferroelectric domains were polarized by applying a voltage between a metallized AFM tip and the substrate as the tip was scanned over the surface. The written areas were then imaged by oscillating the AFM cantilever at its resonant frequency (~70 kHz) while scanning the tip at a lift height of 300 to 500 Å (*11*). Electrostatic forces between polarized areas and the tip change the resonant frequency, or, equivalently, shift the phase response of the cantilever, which is measured. To enhance the contrast of the images, we sometimes applied a small tip bias of +1 V or –1 V. The AFM has been used in related ac resonance techniques to observe charging in polymers, as well as to examine and polarize domains in bulk ferroelectric crystals and polycrystalline thin films (*5–7*).

To determine the conditions under which ferroelectric domains can be polarized and imaged, we first took an as grown PZT film and imaged the electric field distribution of the surface over a 12 μm by 15 μm region to establish a baseline measurement. No phase shifts were observed in this image, presumably because of electrostatic passivation of the ferroelectric domains in the film. We then wrote a 10 μm by 10 μm area inside this 12 μm by 15 μm region by scanning the surface with an applied tip bias that was ramped continuously from –10 V at the beginning (left) of the scan to +10 V at the end (right) of the scan. The resulting phase image over the original region, taken with a tip bias of ~1 V, is shown in Fig. 2. Outside of the written 10 μm by 10 μm area, there are no measurable phase shifts, as expected. In the written area between approximately –4 V and +4 V, there are also no observed phase shifts. In sharp contrast, in the regions written with a tip voltage of greater than ~4 to 5 V, there is a nonzero phase shift whose sign depends on the sign of the writing voltage. The abrupt change in contrast we measure starting at approximately ±4 V is consistent with the signature of ferroelectric domain switching and is difficult to explain in the context of simple electrostatic charging (the interpretation of the sign is discussed below). Although for this 1000 Å thick film the coercive voltage should only be 1 V, because of the extremely large dielectric constant of PZT a gap or surface layer of a few angstroms (which is also the roughness of the film) between the tip and the PZT surface is sufficient to increase the required switching voltage to 4 to 5 V, as has been observed in other studies (*6*).

Having established the parameters for writing and imaging of this film, we moved to another part of the film that had been previously untouched. After imaging the surface over a 15 μm by 15 μm area to ensure an absence of incipient phase contrast, we wrote a 10 μm by 10 μm square with +12 V applied to the tip to create a large, uniformly polarized background region, followed by three lines written inside this square with writing voltages of –5, –7, and –9 V. The resulting phase image over the original 15 μm by 15 μm area is shown in Fig. 3; during acquisition of this image, the tip was electrically grounded. As is evident, the 10 μm by 10 μm square appears as a depression in the film, whereas the three lines appear as protrusions in the square, although they still lie below the zero level defined by the unwritten areas. The magnitude of the contrast of each of the lines is similar, with linewidths ranging from 3500 to 6000 Å and the largest line having been written with the highest voltage. This phase image persists for a few hours, although it fades considerably during this time because of stray charge accumulation. In topography, the surface is featureless after writing, the same as what we measure initially.

Because the tip was electrically grounded for this image, allowing charge to flow freely to and from the tip, the electrostatic interaction between the tip and square is attractive because of the appearance of image charges in the tip. This attractive electrostatic force decreases the resonant fre-

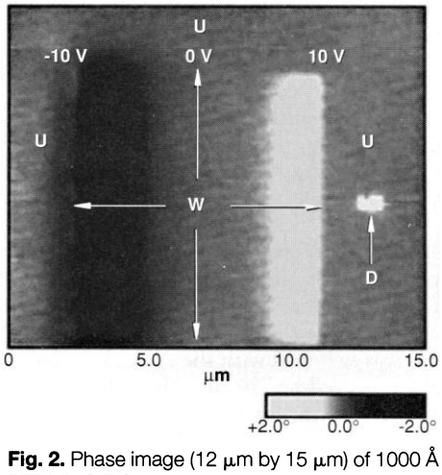

Fig. 2. Phase image (12 μm by 15 μm) of 1000 Å PZT/Nb-$SrTiO_3$ after writing a 10 μm by 10 μm area with a tip bias that was ramped continuously from –10 V at the left of the square to +10 V at the right of the square. The image was acquired with a tip bias of ~1 V. Written and unwritten areas are denoted W and U, respectively; at the right of the image is a dust particle (D).

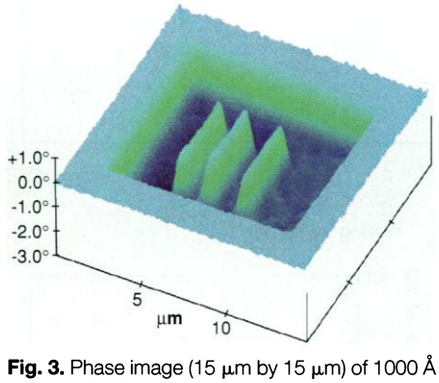

Fig. 3. Phase image (15 μm by 15 μm) of 1000 Å PZT/Nb-$SrTiO_3$ after writing three lines with tip biases of –5, –7, and –9 V (from right to left) inside a square written with +12 V. The square, which appears as a depression in the film, is the result of electrostatic attraction between the grounded tip and sample; the three lines appear as protrusions in the square.

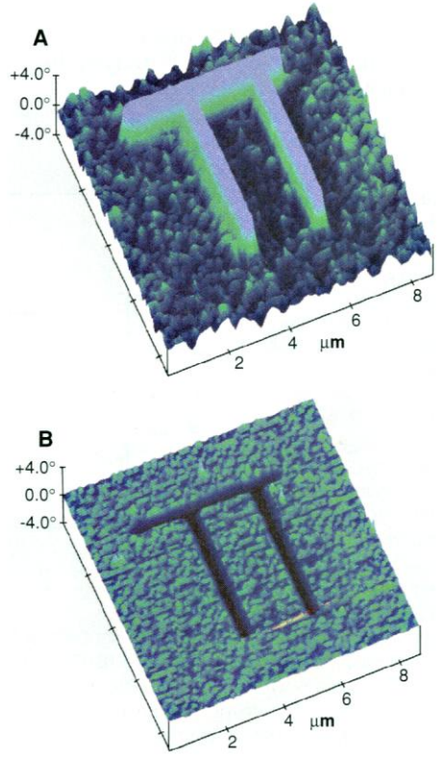

Fig. 4. (**A**) Phase image of a structure written with –12 V inside a square written with +12 V. A reading bias of –1 V was applied during acquisition of the image. (**B**) Phase image of the surface described in (A), acquired with a tip bias of +1 V. The reversal of contrast demonstrates that the features result from electrostatic forces.

quency of the cantilever, resulting in a negative phase shift and hence a depression in the phase image (*12*). In contrast, the lines appear as protrusions in the square because the amount of image charge induced on the tip by the square is reduced in the vicinity of the oppositely polarized lines, resulting in a smaller negative phase shift.

To control whether the electrostatic interaction between the tip and sample is attractive or repulsive, we also acquired images with a reading bias of +1 V or –1 V applied to the tip. In Fig. 4, we show another structure, consisting of two parallel lines connected by a third one, written with –12 V applied to the tip, inside a square written with +12 V to create a uniform background. In the phase image taken with a reading bias of –1 V (Fig. 4A), this structure appears as a protrusion, whereas with a reading bias of +1 V, it appears as a depression (Fig. 4B). This reversal of contrast with bias voltage demonstrates that all of the written features are indeed electrostatic in origin, revealing the charge distribution on the surface of the film (*13*). These experiments give a clear signature of the written areas and demonstrate the ability to polarize as well as switch domains in a controlled, reversible fashion over areas of several square micrometers with submicrometer resolution. We attribute this control over the writing process to the extremely high surface quality of these films.

We next applied this writing procedure to investigate local electronic doping of $SrRuO_3$ in a PZT (4000 Å)/$SrRuO_3$ (30 Å) heterostructure, as shown schematically in Fig. 1. In this experiment, local changes in the PZT polarization produced by the AFM induced a field effect in the conducting $SrRuO_3$ layer 4000 Å below, modifying its carrier concentration and hence its conductivity, which was measured with standard four-point probes. For the purposes of this experiment, the heterostructure was first patterned into a resistivity path 5 μm wide and 15 μm long, and the AFM was used to selectively pole certain areas of this structure with a tip bias of either +14 V or –14 V (inset, Fig. 5A). At the start of the experiment, regions A, B, and C had all been written with a bias of +14 V applied to the tip, effectively writing the entire channel with +14 V. After the resistance of the heterostructure was measured, area A (5 μm by 5 μm) was written with a bias of –14 V, followed by areas B and C. After writing each area, the resistance was measured, and an increase was observed each time. The resistance changes were stable for up to 3 hours, the longest time that we waited. Area B was then poled again with –14 V, and no change in resistance was observed. The structure was then sequentially poled in reverse fashion with a tip bias of +14 V, this time resulting in a drop in resistance after each area was written. At the end, area B was repoled with +14 V, and again no change was observed. Afterward, this area was written with alternating bias voltages of +14 V and –14 V several times to examine the reproducibility of the writing process (*14*).

All of the observed changes in resistance are consistent with the observation of a nonvolatile ferroelectric field effect in the PZT/$SrRuO_3$ heterostructure that occurred only where the AFM had been used to locally switch the polarization of the PZT layer. The sign of the changes we measured agrees with earlier ferroelectric field effect work on $SrRuO_3$ with a conventional Pt metal electrode to switch the PZT polarization, as well as with Hall effect work, which reveals n-type (electron) conductivity in this material (*4*). We also measured how the resistance of area B changed as a function of the magnitude of the writing voltage used. Figure 5B shows the measured change in resistance as area B was written with different voltages. Above 8 V, resistance changes were observed that are basically independent of the magnitude of the writing voltage, whereas below 8 V, there was essentially no resistance change as a function of writing voltage, consistent with a ferroelectric field effect.

Our measurements of quantitative changes in resistance are also revealing. The total size of the effect is ~3% for the entire path. In earlier work on PZT/$SrRuO_3$ (30 Å) heterostructures with a conventional metal electrode for poling, we measured a resistance change as large as 9%. The reason for the discrepancy between the two measurements is that the structure measured in this experiment is not in fact a true four-point resistivity path because of the presence of contact resistance. By assuming that the intrinsic resistivity of this sample is the same as that used in previous work, 1.2×10^{-3} ohm·cm, and by subtracting out the calculated contact resistance, we estimate the size of the effect over the written regions to be ~8%, corresponding to a change in sheet resistance of 300 ohms per square.

For a PZT/$SrRuO_3$ (30 Å) heterostructure whose geometry was suitable for four-point resistivity measurements, a resistivity of 1×10^{-3} ohm·cm was found. When the polarization of the entire path (5 μm by 5 μm) was switched with the AFM, the resistivity changed by 7%, near the value of 9% observed in earlier work. The agreement between these two experiments, which used different methods to switch the polarization of the PZT layer, shows that the AFM is effective in switching the ferroelectric polarization. Indeed, one concern with this local poling approach is that written domains may not extend uniformly in the vertical direction all the way down to the $SrRuO_3$ film, as

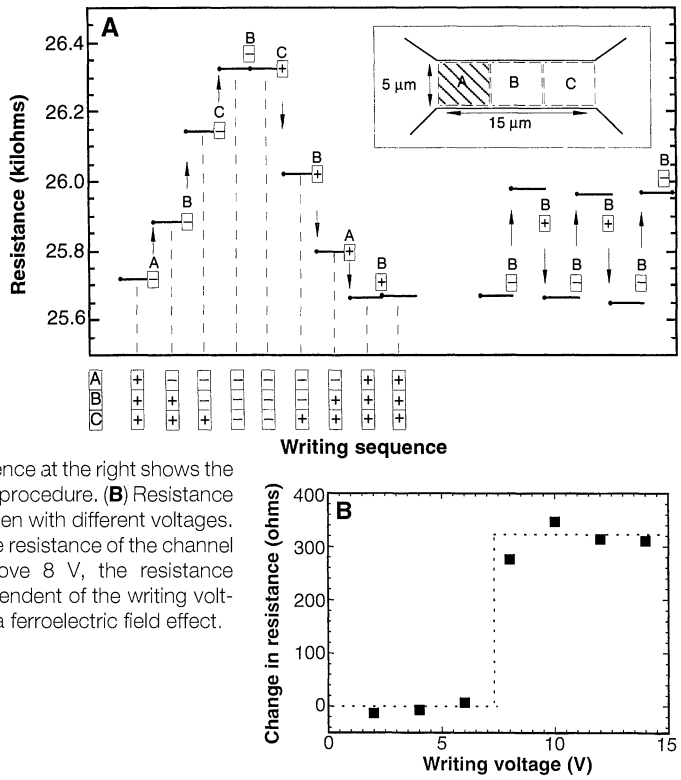

Fig. 5. (**A**) Resistance as a function of area written by the AFM tip for the structure shown schematically in the inset. The horizontal axis denotes the polarization state of the various portions of the structure, and the letters A, B, and C indicate points at which individual areas were written, with the + or – signs indicating whether an area was written with +14 V or –14 V. The staircase demonstrates local, reversible switching behavior, and the sequence at the right shows the reproducibility of the poling procedure. (**B**) Resistance change as area B was written with different voltages. Below 8 V, no change in the resistance of the channel is observed, whereas above 8 V, the resistance change is essentially independent of the writing voltage used, consistent with a ferroelectric field effect.

has been seen in related optical studies of $MgO:LiNbO_3$ ferroelectric crystals (*15*). The electric field images presented earlier, though revealing and self-consistent, cannot address this question. However, the field effect—a direct measure of ferroelectric switching—gives a clear answer. The observed change in resistance of the $SrRuO_3$, lying 4000 Å below the level where the AFM had been used to write, indicates uniform switching of the ferroelectric polarization in the vertical direction. Finally, we have also used this structure to show that this writing procedure can be performed down to dimensions of 3500 Å. A 3500 Å wide line, whose width was determined from phase imaging, was traced along the length of the structure, resulting in a 0.5% change in the resistance. The calculated percent change is also 0.5%. Writing wider lines (8500 Å and 1.35 μm) revealed larger resistance changes that also scaled with area.

In principle, our method should enable the writing of electronic features as small as the radius of curvature of the AFM tip, a few hundred angstroms; recently, features as small as 1700 Å have been written (*16*). This approach is generally applicable to many classes of materials, given the strong progress that has been made in the thin-film deposition of epitaxial oxide films. It can be applied directly to many perovskite oxide systems, including the high-temperature superconductors, to investigate superconducting field effect devices as well as Josephson field effect devices and arrays (*17*). Also, because the heteroepitaxial growth of ferroelectric PZT, $BaTiO_3$, and related oxides has been demonstrated on single-crystal Si and GaAs, it should be possible to extend this approach to semiconductor structures, where the carrier densities are orders of magnitude smaller than in $SrRuO_3$ (*3*, *18*).

REFERENCES AND NOTES

1. J. F. Scott and C. A. Paz de Araujo, *Science* **246**, 1400 (1989).
2. R. Ramesh *et al.*, *ibid.* **252**, 944 (1991); C. B. Eom *et al.*, *ibid.* **258**, 1766 (1992); C. H. Ahn *et al.*, *ibid.* **269**, 373 (1995); Y. Watanabe, *Appl. Phys. Lett.* **66**, 1770 (1995).
3. C. B. Eom *et al.*, *Appl. Phys. Lett.* **63**, 2570 (1993).
4. C. H. Ahn *et al.*, *ibid.* **70**, 206 (1997).
5. F. Saurenbach and B. D. Terris, *ibid.* **56**, 1703 (1990); R. Lüthi *et al.*, *J. Appl. Phys.* **74**, 7461 (1993).
6. T. Hidaka *et al.*, *Appl. Phys. Lett.* **68**, 2358 (1996).
7. J. E. Stern, B. D. Terris, H. J. Mamin, D. Rugar, *ibid.* **53**, 2717 (1988).
8. J. Massanell, N. Garcia, A. Zlatkin, *Opt. Lett.* **21**, 12 (1996); O. Kolosov *et al.*, *Phys. Rev. Lett.* **74**, 4309 (1995).
9. C. H. Ahn *et al.*, in preparation. The deposition rate was ~5 Å s^{-1} and the substrate temperature was held at 660°C, with atomic oxygen provided to the sample at a background pressure of 2×10^{-5} torr.
10. J.-M. Triscone *et al.*, *J. Appl. Phys.* **79**, 4298 (1996). The deposition rate was ~0.1 Å s^{-1}, and the substrate temperature was held at 530°C, with a background pressure of 0.2 torr of oxygen and argon (P_{O_2}/P_{Ar} = 40%).
11. The nominal radius of curvature for the metallized tips used in this experiment is ~500 Å, and the spring constant is 1 to 5 N m^{-1}. The tip amplitude used was ~300 Å.
12. In this grounded mode of operation, the response of the cantilever is invariant to the polarity of the ferroelectric, always being attractive. Squares written with positive voltages appear as depressions, as do squares written with negative voltages.
13. The sign of the observed contrast in these images for a given reading bias shows that the electrostatic interaction between the tip and surface results from an overscreening of the surface after the ferroelectric polarization has switched, similar to what is observed in electret materials with aligned dipolar moments [G. M. Sessler, Ed., *Electrets* (Springer-Verlag, Berlin, 1980)]. From the bias voltage needed to reverse the contrast of these images (<1 V magnitude), we estimate that this excess screening charge density represents a small fraction (<1%) of the induced ferroelectric polarization charge density.
14. We believe that area B gave the most reproducible changes in resistance because there were a few dust particles present on the otherwise featureless surface, making it easier to locate the same area for poling. Areas A and C were more difficult to locate reproducibly, and the variations in step height for the staircase in Fig. 5A may be largely attributable to difficulties in locating exactly the same areas, potentially leading to overlap between the poled regions.
15. A. Kuroda, S. Kurimura, Y. Uesu, *Appl. Phys. Lett.* **69**, 1565 (1996).
16. T. Tybell *et al.*, in preparation.
17. J. Mannhart, *Supercond. Sci. Technol.* **9**, 49 (1996).
18. K. Nashimoto, D. K. Fork, T. H. Geballe, *Appl. Phys. Lett.* **60**, 1199 (1992).

19. We thank M. Decroux, S. R. Manalis, L. Miéville, S. C. Minne, C. F. Quate, J. W. Reiner, and S. Reymond for useful discussions and technical advice. Supported by the Swiss National Science Foundation and the U.S. Air Force Office of Scientific Research.

21 January 1997; accepted 17 March 1997

Disordered Biopyriboles, Amphibole, and Talc in the Allende Meteorite: Products of Nebular or Parent Body Aqueous Alteration?

Adrian J. Brearley

Transmission electron microscope observations of the Allende carbonaceous chondrite provided evidence of widespread hydrous phases replacing enstatite in chondrules. Calcic amphibole and talc occur in thin (less than 0.3 micrometer) crosscutting veins and as alteration products of primary chondrule glass in contraction cracks within the enstatite. In addition, talc and disordered biopyriboles were found replacing enstatite grains along cracks and fractures. Although rare hydrous phases have been reported in calcium- and aluminum-rich inclusions in the Allende meteorite, these observations suggest that aqueous fluids played a much more significant role in the mineralogical and geochemical evolution of Allende than has previously been thought.

Carbonaceous chondrites are among the most primitive of solar system materials and provide important clues into processes such as evaporation, condensation, and melting, which took place in the earliest stages of the formation of our solar system (*1*). Many carbonaceous chondrites have experienced aqueous alteration at low temperatures (*2*), but the location and timing of these reactions are controversial. For example, the rare hydrous phases found in some calcium- and aluminum-rich inclusions (CAIs) and chondrules (*3–7*) in the Allende CV3 carbonaceous chondrite have been attributed to both preaccretionary (nebular) and postaccretionary (parent body) (*7*) hydrous alteration reactions. A resolution of the timing and location of aqueous alteration would improve our understanding of nebular processes and the evolution of the parent bodies of carbonaceous chondrites.

This study reports high-resolution transmission electron microscope (HRTEM) observations of pyroxene-rich chondrules in Allende, which show that the effects of aqueous alteration are more widespread than previously recognized. Seven porphyritic pyroxene chondrules from a single thin section of Allende were selected for study by TEM (*8*). In all seven chondrules, the dominant phase is clinoenstatite ($En_{93-98}Wo_1$), with subordinate olivine (Fa_{1-10}) sometimes constituting up to 30 modal percent of the chondrule (Fig. 1). The clinoenstatite in all three chondrules has been extensively replaced by FeO-rich olivine (Fa_{29-45}) (*9–12*), and primary MgO-rich olivines invariably have narrow rims (<15 μm) of FeO-rich olivine surrounding them. Glass in all chondrules has been replaced by a fine-grained (<50 μm) assemblage of minerals that were not studied in detail but include nepheline and sodalite (*13*).

Analysis by HRTEM showed that the development of hydrous phases is widespread in all seven chondrules but is consistently restricted to the phenocrysts of

Institute of Meteoritics, Department of Earth and Planetary Sciences, University of New Mexico, Albuquerque, NM 87131, USA.